Semi-Automatic Matching of OCT and IVUS Images For Image Fusion

Olivier Pauly[a], Gozde Unal[a], Greg Slabaugh[a], Stephane Carlier[b], Tong Fang[a]

[a]Siemens Corporate Research, Princeton, NJ, USA
[b]Cardiovascular Research Foundation, New York, USA

ABSTRACT

Medical imaging is essential in the diagnosis of atherosclerosis. In this paper, we propose the semi-automatic matching of two promising and complementary intravascular imaging techniques, Intravascular Ultrasound (IVUS) and Optical Coherence Tomography (OCT), with the ultimate goal of producing hybrid images with increased diagnostic value for assessing arterial health. If no ECG gating has been performed on the IVUS and OCT pullbacks, there is typically an anatomical shuffle (displacement in time and space) in the image sequences due to the catheter motion in the artery during the cardiac cycle, and thus, this is not possible to perform a 3D registration. Therefore, the goal of our work is to detect semi-automatically the corresponding images in both modalities as a preprocessing step for the fusion. Our method is based on the characterization of the lumen shape by a set of Gabor Jets features. We also introduce different correction terms based on the approximate position of the slice in the artery. Then we train different support vector machines based on these features to recognize these correspondences. Experimental results demonstrate the usefulness of our approach, which achieves up to 95% matching accuracy for our data.

Keywords: Atherosclerosis, Optical Coherence Tomography, Intravascular Ultrasound, Matching, Pattern Recognition, Feature Extraction, Machine Learning, Registration

1. INTRODUCTION

In western countries, atherosclerosis is the major cause of sudden death or disability. A sudden death is related to the disruption of atheromatous lesions called vulnerable plaque on the blood vessel wall of the coronary artery. Unfortunately these are not visible with angiography, the most commonly used investigation technique. Intravascular Ultrasound (IVUS) is regarded by many physicians as the gold standard in atherosclerosis diagnosis.[1] This is a catheter-based imaging modality with a large penetration depth. But the drawback of this technique is its comparably poor resolution. A relatively new catheter-based imaging technology named Optical Coherence Tomography (OCT) uses light interference to offer in contrary a very good resolution for a small penetration depth.

Clinical studies have shown that fibrous cap thickness or protruding plaque fractures are hardly determinable with IVUS in contrary to OCT. OCT can help to identify these minor or silent plaques that carry the risk of thrombosis resulting in sudden death.[2] Other studies released by Volcano Corporation have shown that IVUS associated with Virtual Histology (VH) can provide the composition of the vulnerable plaque.[3] Because the features of the two imaging modalities IVUS and OCT are complementary, the combination of the information they provide would permit an increased diagnostic value for assessing arterial health and for the monitoring of atherosclerosis.

An interesting approach of fusion of OCT and IVUS images based on landmarks extraction was presented by Unal et al.[4] First the corresponding OCT and IVUS images are manually selected. Then landmarks like side-branch or calcification are semi automatically detected. The image is transformed in the rectangular domain, and then the thickness of the vessel wall is evaluated over the entire scan. The lumen contour and the detected farthest field contour are segmented, and the distance in between is computed for each column. The locations

Further author information: (Send correspondence to Gozde Unal or Olivier Pauly)
Gozde Unal: E-mail: gozde.unal@gmail.com
Olivier Pauly: E-mail: olivier.pauly@gmail.com

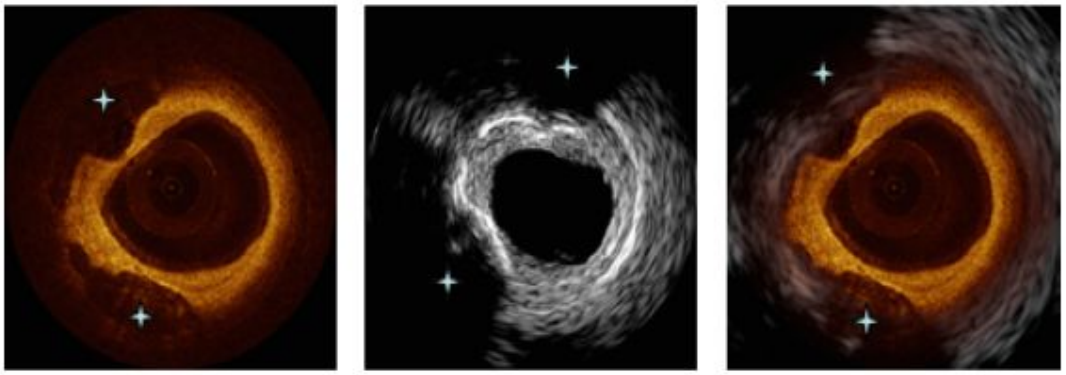

Figure 1. Here is an example of the fusion of an OCT (on the left) and an IVUS (in the middle) cross sectional image, *image courtesy of G. Unal et al.*

where this distance sinks dramatically under the average thickness of the wall corresponds to a landmark. After locating these landmarks, a rigid registration is performed to align them in both images. For refinement a non-rigid registration is performed to account for local deformations. A highly smoothed gradient image is used as a similarity metric with the normalized cross correlation as statistical similarity measure. Finally the images can be fused in a weighted way based on anatomical information and advantages of each modality. An example of registration can be seen on Figure 1. The limitation of this technique is that specific landmarks are required to perform the fusion. And these are not present in each slice from an IVUS or OCT pullback. For example, landmarks like calcification are visible with IVUS but not always with OCT.
The goal of our work is to develop a computer algorithm which could perform the fusion of IVUS and OCT with a contour-based technique. The first idea would be to perform a 3D registration of the IVUS and OCT volumes. But studies have shown that during a motorized 0.5 mm/s catheter pullback, there is an anatomical shuffle (in time and space) in the investigation due to the catheter displacement in the blood vessel during the cardiac cycle.[5] Thus, if there is no ECG gating such as the Intelligate method described in the paper by S. A. de Winter et al.,[5] the registration can only be performed between the 2D images. The first step is the segmentation of the lumen contour in each slice on IVUS and OCT pullbacks from the same patient. Then we perform the semi-automatic matching of corresponding slices. Therefore we want to extract features from the lumen contour shape to characterize an image and to be able to compare it with images from the other modality. The challenge will be to extract adequate features that take into account small deformations of the lumen or other orientations of the probe in the artery. With support vector machines, we will test different features and different parameters to build the optimal 'matcher' for our problem.

2. SEGMENTATION OF THE LUMEN SHAPE

The automatic segmentation of the blood vessel wall in IVUS images has always been a very difficult problem because of the amount of noise and artefacts in the images. The most commonly used techniques are based on active contours (snakes) and gradient vector flow (GVF).[6] A snake deforms itself under the influence of external forces (the GVF in this case), and of internal forces such as elasticity, rigidity, viscosity or pressure in order to find the boundaries of an object. The use of GVF increases the capture range of the active contour, so that it can find the boundaries even if they are far from the snake's initial position. This also prevents the snake from getting stuck because of noise or catheter artifacts.
Let us briefly explain the segmentation methods we used to extract the lumen contour before performing the feature extraction. First we use a shape-driven segmentation to extract the lumen contour described by G. Unal et al. [7] A statistical shape space is built in which each shape is represented by a vector of weights. The evolution of the active contour is defined by an energy minimization using a global intensity model. An example of segmentation can be seen on the images in Figures 2 and 3. For the very challenging cases where this method failed, we use a semi automatic method based on Hermitian splines.

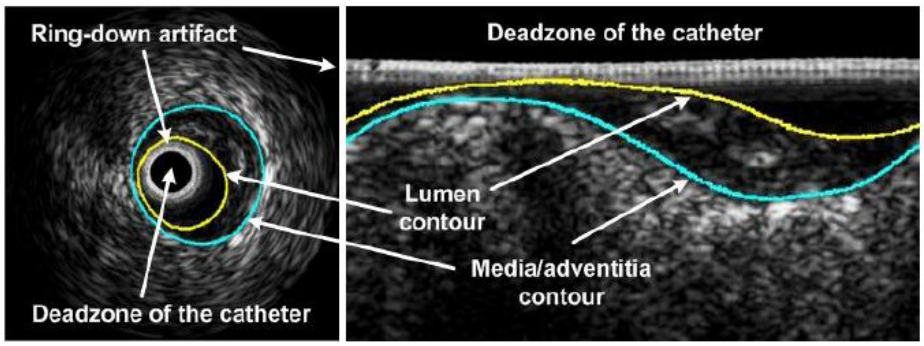

Figure 2. Shape-driven Segmentation of IVUS images. An elegant approach for lumen contour segmentation in IVUS images, *image courtesy of G. Unal et al.*

The lumen contour in OCT images in contrast to IVUS, can be easily segmented with more conventional segmentation techniques that we will not describe in this paper. The next step is to extract several features from these contours to characterize the shape of the lumen.

3. FEATURE EXTRACTION

In this section, we present the features extracted from the lumen contour of OCT and IVUS images (see Figure 5). The goal is to characterize the shape of the lumen with efficient descriptors.

3.1 Gabor Jets

The Gabor Jets are defined as the responses of an image filtered by a set of Gabor filters. They received particular attention in computer vision because characteristics of cells in the visual area of the cortex of some mammals can be approximated by these filters.[8] A Gabor filter can be viewed as a sinusoidal plane modulated by a Gaussian envelope:

$$h(x,y) = s(x,y)g(x',y') \tag{1}$$

where $s(x,y)$ is a complex sinusoid called carrier, $g(x,y)$ is a 2D Gaussian envelope, $x' = x\cos\theta + y\sin\theta$, and $y' = -x\sin\theta + y\cos\theta$. θ is the orientation of the filter. The sinusoid is defined as following:

$$s(x,y) = \exp(-j2\pi(u_0x + v_0y)) \tag{2}$$

The Gaussian envelope is:

$$g(x,y) = \frac{1}{\sqrt{2\pi}\sigma_x\sigma_y}\exp(-\frac{1}{2}(\frac{x^2}{\sigma_x^2} + \frac{y^2}{\sigma_y^2})) \tag{3}$$

Thus the Gabor filter is defined as:

$$h(x,y) = \exp(-\frac{1}{2}(\frac{x'^2}{\sigma_x^2} + \frac{y'^2}{\sigma_y^2}))\exp(-j2\pi(u_0x + v_0y)) \tag{4}$$

In our case, we will create a battery of Gaussian filters with 4 different orientations (θ) and 16 different scales (σ_x, σ_y).[9] We apply these filters on the extracted lumen contour as shown in figures 6. Then a local maximum operation is computed over scale and position to get a set of feature images.

3.2 Local Maximum Operation

After applying the battery of Gabor filters on our contour, we obtain N image responses (N is chosen even). We perform on a $(k, k+1)$ (with $k \in [1, N-1]$) pair of image responses a local maximum operation.
Let us first define a $M \times M$ neighborhood window centered on each pixels (i,j) in image k and image $k+1$. The pixel (i,j) in the resulting image will receive the maximum intensity value contained in the both areas defined by the windows in image k and image $k+1$ (see images 7). This operation gives us finally our $N/2$ shape descriptors.

h

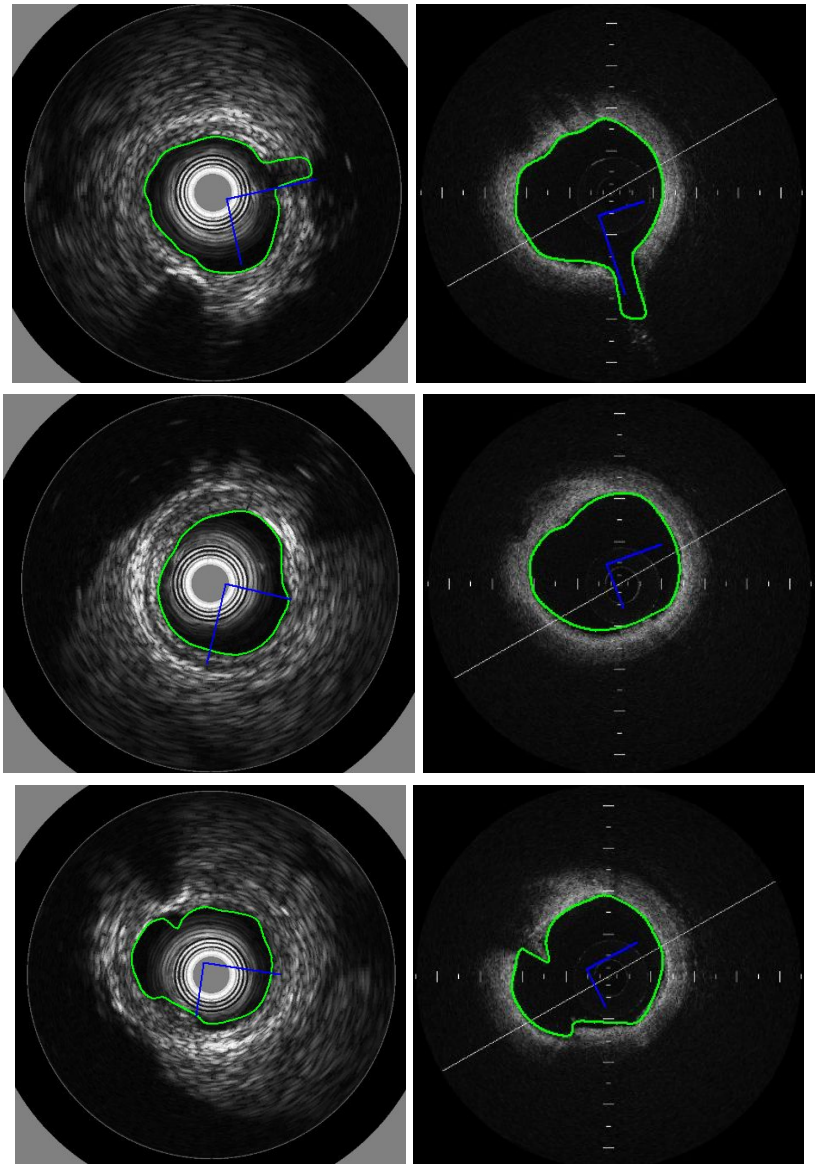

Figure 3. Segmentation of corresponding OCT and IVUS images. In the first row, a side-branch can be seen on both modalities, where this feature is reflected by a protrusion in the contour. In the second row, a small calcification can be seen near the lumen contour, characterized by a higher intensity and a shadowing effect. This feature is easier to detect on the IVUS than on the OCT image. In the third row, the beginning of a bifurcation of the vessel can be seen on both images.

3.3 Discussion

Correspondences between IVUS and OCT frames are not easily recognizable because the probe can have a different trajectory in the artery during the acquisition pullback. The acquisition time can be also at a different point in the cardiac cycle, so that the artery is more or less deformed. Our goal is to compare the ability of different features to characterize the shape of the lumen contour for accurate matching. The next step is to test the ability of our Gabor Jets features with a machine learning approach to recognize correspondences between OCT and IVUS images.

4. MATCHING APPROACH

In this section, we describe our approach to perform the matching between OCT and IVUS images from the same patient.

4.1 The Matcher, a One-Class Support Vector Machine

In Machine Learning, Support Vector Machines (SVM) show very attracting features such as efficiency, computation speed and capacity to find an optimal hyperplane for nonseparable patterns[10].[11] But it is always difficult to tune the SVM for an optimal learning avoiding the problems of overfitting the training data. It is also possible to choose between different inner-product kernels like polynomial or radial-basis functions. These kernels are used to map the input features to a higher-dimensional space and thus to increase the separability of patterns. In the case of the Gabor Jets, we use the following procedure:

1. Perform a rigid registration on the contours
2. Apply the battery of Gabor filters
3. Perform the maximum operation
4. Compute the mutual information between each feature images

We define the input vector V_{input} to our matcher as:

$$V_{input}(i) = MI(I_{OCT}(i), I_{IVUS}(i))\,, \tag{5}$$

where MI is the mutual information of the feature images I_{OCT} and I_{IVUS} (obtained as explained in Section 3).
We want also to introduce a correction parameter taking into account the supposed position of the slice in the artery. The mutual information is modulated by a term depending of the pullback speed and the acquisition frequency of the imaging modality. We are not able to determine the exact position of the slice in the artery because of the anatomic shuffle due to the heartbeat of the patient. But we can still dismiss the correspondence candidates that are too far from each other. Let us introduce first a simple non-linear correction:

$$V_{input}(i) = (1-\gamma)MI(I_{OCT}(i), I_{IVUS}(i))\,, \tag{6}$$

with:

$$\gamma = \frac{\frac{(i-r)}{f} \cdot v}{L} \tag{7}$$

where i is the current slice number, r is a reference correspondence given by the user as input, f is the acquisition frequency in Hz, v the pullback speed in mm/s, and L is the length of the longest pullback in mm (used here as a normalization parameter). We can also introduce another non-linear correction:

$$V_{input}(i) = \frac{2}{\pi} atan(\alpha\gamma) MI(I_{OCT}(i), I_{IVUS}(i))\,, \tag{8}$$

where γ is the same as described before, and α is a parameter that has to be tuned to increase the selectivity of this correction term.
We choose a One-Class Support Vector Machine (SVM) for our matching problem: the label associated to a correspondence is 1 and the one associated to non-correspondence is -1. During the training, the SVM will construct an optimal hyperplane to separate these patterns as shown in Figure 4.

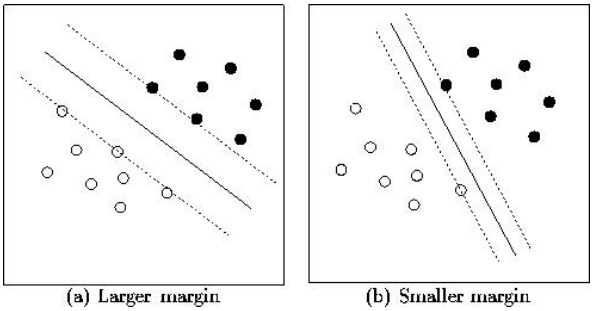

Figure 4. The Support Vector Machine will construct an optimal hyperplane to separate the correspondences (here in white for example) from the non-correspondences (here in black)

4.2 Measure of the performance of a matcher

To measure and to improve the performance of matching, we use the receiver operator characteristic (or ROC). This is basically the plot of the sensitivity vs. (1 - specificity), or equivalently the fraction of true positive vs. the fraction of false positive. First it helps us to choose the best threshold of decision for our matchers, and then we are able to compare different matchers based on different features.

4.2.1 Confusion Matrix and ROC space

The role of the matcher is to classify the inputs in two categories: the correspondences (positive), and the non-correspondences (negative). We can distinguish four outcomes of a prediction:

- True positive (hit), i.e. the matcher classifies the pair as a correspondence, and this is a real correspondence.
- False positive (Type I error), i.e. the matcher classifies the pair as a correspondence, but this is not a correspondence.
- True negative (correct rejection), i.e. the matcher classifies the pair as a non-correspondence, and this is a not a correspondence.
- False negative (Type II error), i.e. the matcher classifies the pair as a non-correspondence, but this is a real correspondence.

To draw our ROC curve, we need to compute the True Positive Rate (TPR) and the False Positive Rate (FPR). The TPR determines the performance of the matcher to detect the correspondences among all the correspondences contained in the test samples. It is also defined as sensitivity. The FPR defines on the other hand the non-correspondences incorrectly detected as correspondences among all the non-correspondences in the test samples. This is equivalent to (1-specificity). The ROC curve also maps each matcher to one point (TPR, FPR) in the ROC space.

4.2.2 Finding the best threshold of decision for one matcher

After the training of the matcher, we have to find the best decision threshold for our application. In fact the matcher predicts values that are not just 1 for a correspondence or -1 for a non-correspondence. So we have first to determine the range of predicted values by using a test stack of correspondences and non-correspondences. Let p_1 and p_2 respectively be the lowest and the uppest predicted values. Our threshold T is in the interval $[p_1, p_2]$. For each $T \in [p_1, p_2]$, the TPR and the FPR of the matcher is computed and reported on a ROC curve.

Figure 5. Extraction of the lumen contour in an OCT image

Figure 6. Gabor Jets Extraction of OCT Lumen shape by filtering the OCT contour with a battery of Gabor filters

4.2.3 Comparing the different matchers

The ROC curve can also be used to compare the matchers using different set of features. There are different ways of identifying the optimal matcher: the ROC convex hull, the area under curve (AUC) and the accuracy. If you draw the ROC curve for one matcher (see precedent section), the AUC is the integral of this curve. By drawing the ROC curves of several matchers on the same graph, it is possible to find the convex hull of all these curves. A matcher belonging to this hull is an optimal matcher.[12] In our case, we compute for each matcher the area under curve and the accuracy.

5. RESULTS

The different sets of features chosen were the simple Gabor Jets, the Gabor Jets with simple non-linear correction, and the Gabor Jets with atan non-linear correction. The pullback speed was 1 mm/s and the acquisition frequency was chosen 1Hz for both modalities. In the atan non-linear correction, α was heuristically chosen equal to 20. We chose a linear kernel for our different One-Class SVM and trained them with a training set of 20 pairs of OCT-IVUS images containing 10 correspondences. We tested them with a test set of 100 pairs also containing 10 correspondences. The results can be seen in the Table 1. The accuracy of the matcher is 87.4% with the simple Gabor Jets, 88.2% with the simple non-linear correction and 95.0% with the atan non-linear correction. The ROC curve of the Gabor Jets can be seen on the Figure 8.

True positive and false positive examples are shown on the Figures 9 and 10 respectively. In the true positive examples, strong features like side-branch lead to success. In the false positive examples, contours had weak descriptive features for discrimination, and because of the very bad quality of some IVUS pullbacks, a good segmentation and thus a good matching efficiency are much harder to obtain. The simple non-linear or atan non-linear correction terms help the matcher to dismiss some correspondence candidates that should be too far

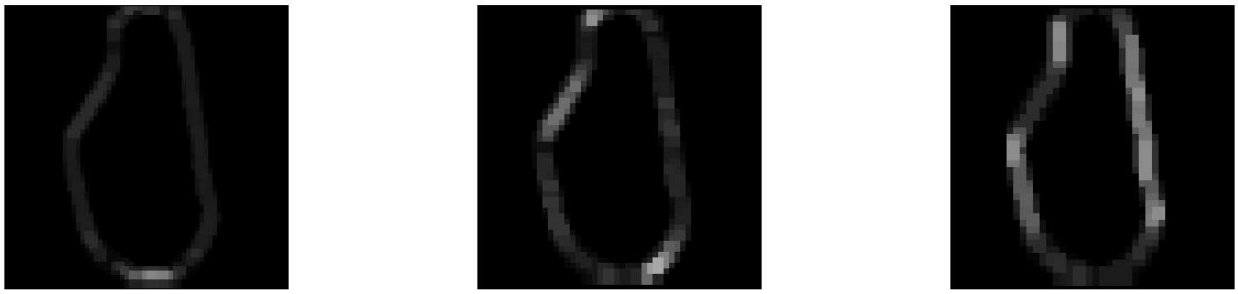

Figure 7. Local maximum operation over scale and position performed on the Gabor Jets images

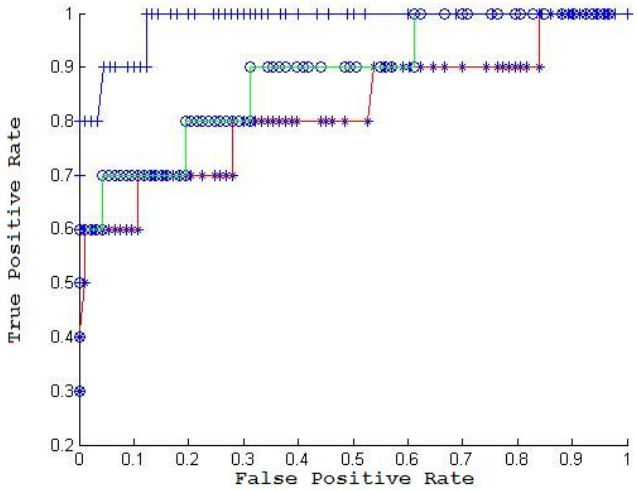

Figure 8. ROC curve of the matchers based on the Gabor Jets features: in red, the matcher is based on simple Gabor Jets; in green, the matcher is based on Gabor Jets with simple non-linear correction; in blue, the matcher is based on Gabor Jets with atan non-linear correction

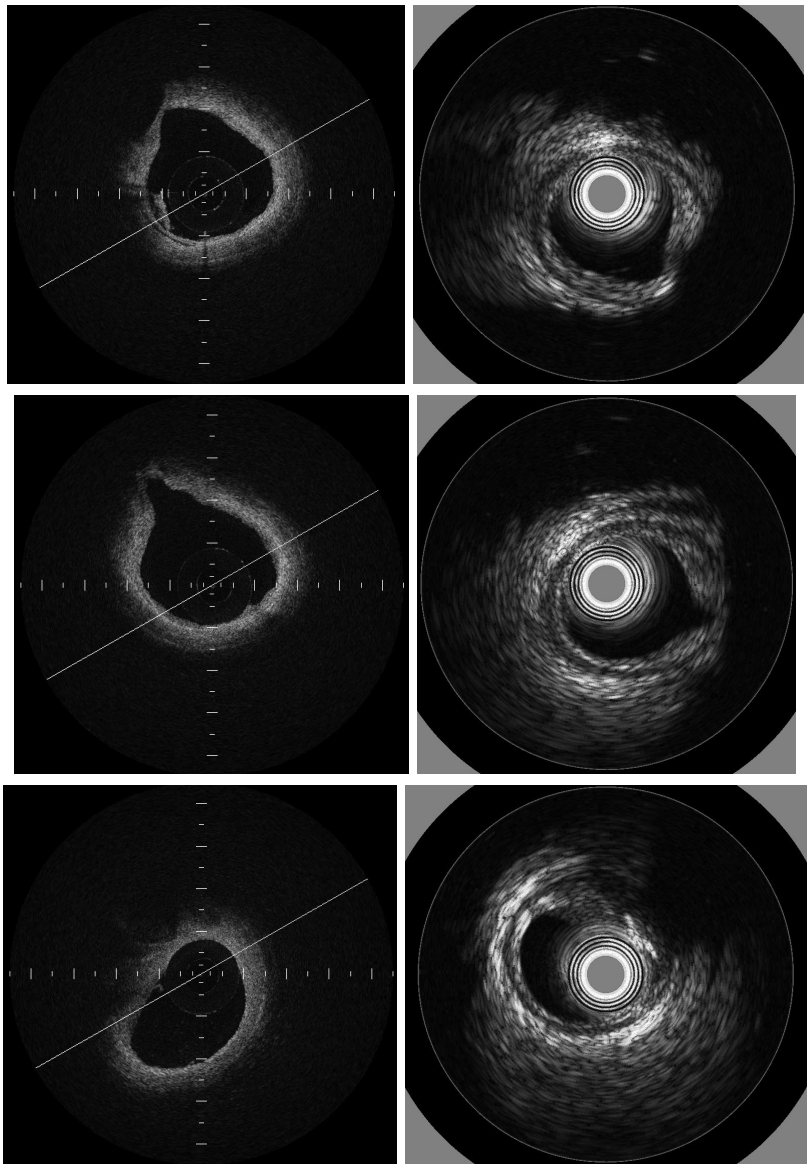

Figure 9. True positive Examples: correctly matched correspondences

Table 1. After training a SVM with each set of features, we compare the created matchers by computing their ROC Curves, Area Under Curve and accuracy.

	Accuracy	AUC (Area Under Curve)
Gabor Jets	87.4 %	0.82
Gabor Jets with simple non-linear correction	88.2 %	0.88
Gabor Jets with atan non-linear correction	95.0 %	0.98

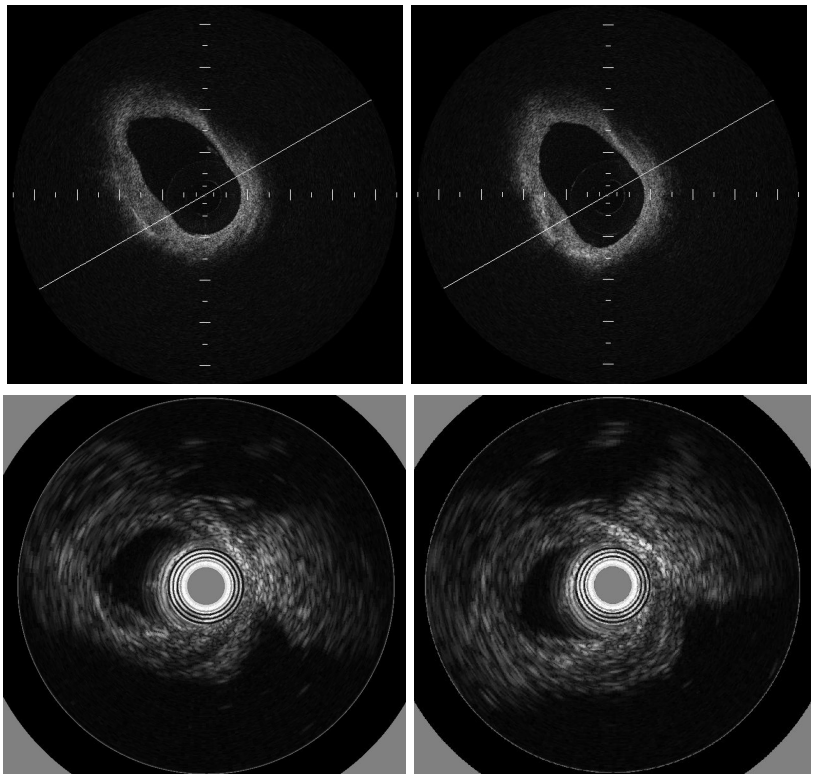

Figure 10. False positive Examples: on top the both OCT images will be cross mismatched with the both IVUS images below

from one another in the artery. This is why the accuracy and the AUC are higher in the case of Gabor Jets with correction. The atan non-linear term has a higher selectivity than the simple non-linear, because of the sharper threshold form of the atan function. In that way we obtain better results with this non-linear correction term. The tuning of α permits to increase or reduce its weight in regard of the mutual information term.

6. CONCLUSION

We implemented a semi-automatic matching of Intravascular Ultrasound and Optical Coherence Tomography images of the coronary arteries from the same patient as a preprocessing step of a registration. The fusion of these modalities provides more information for a better diagnosis and understanding of atherosclerosis. Therefore we considered the lumen shape in these images and extracted different sets of descriptors. We could train and test different SVM based on these different feature sets to recognize the corresponding IVUS and OCT shapes. As shown in the results table, the Gabor Jets with non-linear correction give the best matcher for our test set and the method is robust to translation, rotation, rescaling and small non-linear deformations. The main difficulty in making the right decision is on one hand to recognize two corresponding shapes with small deformations as positive, and on the other hand to reject two non-corresponding shapes that are very similar and with also small

deformations. This is why we introduced correction terms taking into account the approximate position of the slice in the artery. But the tuning of this correction term is crucial because it could reduce the importance of the mutual information term. The size of the training set was unfortunately small so we could not test the generalization ability of our matcher. Future work would be to build a larger training and test set to improve the robustness of the matching by choosing the best compromise between SVM, Gabor Jets and correction terms parameters.

REFERENCES

1. G. Goerge and J. Ge, "Intravasaler ultraschall - der neue goldstandard?," *Zeitschrift fuer Kardiologie* , 1997.
2. U. Gerckens, "Optical coherence tomography (oct),potential of a new high-resolution intracoronary imaging technique," *Herz* , 2003.
3. Volcano, "www.volcanocorp.com,"
4. G. Unal, S. Lankton, and G. Slabaugh, "Fusion of ivus and oct trough semi automatic registration," *Proceedings of MICCAI CVII* , 2006.
5. S. A. de Winter et al., "Retrospective image-based gating of intracoronary ultrasound images for improved quantitative analysis: The intelligate method.," *Catheterization and Cardiovascular Interventions* , 2004.
6. C. Xu and J. L. Prince, "Snakes, shapes, and gradient vector flow," *IEEE Transactions on Image Processing* , 1998.
7. G. Unal, G. Slabaugh, and S. Carlier, "Shape-driven segmentation of intravascular ultrasound images," *Proceedings of MICCAI CVII* , 2006.
8. D. J. Freedman and M. Riesenhuber, "Visual caterogization and the primate prefontal cortex: Neurophysiology and behaviour," 2002.
9. T. Serre and L. Wolf, "Robust object recognition with cortex-like mechanisms," *IEEE Transactions on Pattern Analysis and Machine Intelligence* , 2007.
10. S. Haykin, *Neural Networks, A Comprehensive Foundation*, Prentice Hall, 1999.
11. Z.-H. H. et al., "An empirical comparison of ensemble classification algorithms with support vector machines," *Proceedings of the Third International Conference on Machine Learning and Cybernetics* , 2004.
12. T. Fawcett, "An introduction to roc analysis," *Pattern Recognition Letters* , 2005.